Atmos. Chem. Phys. Discuss., 12, 3467–3507, 2012
www.atmos-chem-phys-discuss.net/12/3467/2012/
doi:10.5194/acpd-12-3467-2012

Atmospheric Chemistry and Physics Discussions

Interaction of anthropogenic and natural emission sources during a wild-land fire event – influence on ozone formation

E. Bossioli[1], M. Tombrou[1], A. Karali[2], A. Dandou[1], D. Paronis[3], and M. Sofiev[4]

[1]Division of Environmental Physics and Meteorology, Department of Physics, National and Kapodistrian University of Athens, Building PHYS-5, Panepistimioupolis, 15784 Athens, Greece
[2]Institute for Environmental Research and Sustainable Development, National Observatory of Athens, I. Metaxa & V. Pavlou, P. Penteli (Lofos Koufou) 15236, Athens, Greece
[3]Institute for Space Applications and Remote Sensing, National Observatory of Athens, I. Metaxa & V. Pavlou, P. Penteli (Lofos Koufou) 15236, Athens, Greece
[4]Finnish Meteorological Institute, Erik Palmenin aukio 1, P.O. Box 503, 00101 Helsinki, Finland

Received: 7 November 2011 – Accepted: 23 January 2012 – Published: 31 January 2012

Correspondence to: E. Bossioli (ebossiol@phys.uoa.gr)

Published by Copernicus Publications on behalf of the European Geosciences Union.

Abstract

The objective of this study is to investigate the contribution of biomass burning in the formation of tropospheric O_3. Furthermore, the impact of biogenic emissions under fire and no fire conditions is examined. This is achieved by applying the CAMx chemistry transport model for a wild-land fire event over Western Russia (24 April–10 May 2006). The model results are compared with O_3 and isoprene observations from 117 and 9 stations of the EMEP network, respectively.

Model computations show that the fire episode altered the O_3 sensitivity in the area. In particular, the fire emissions increased surface O_3 over Northern and Eastern Europe by up to 80 % (40–45 ppb). In case of adopting a high fire NO_x/CO emission ratio (0.06), the area (Eastern Europe and Western Russia) is characterized by VOC-sensitive O_3 production and the impact of biogenic emissions is proven significant, contributing up to 8 ppb. Under a lower ratio (0.025), total surface O_3 is almost doubled due to higher O_3 production at the fire spots and lower fires' NO emissions. In this case as well as in the absence of fires, the impact of biogenic emissions is almost negligible. Injection height of the fire emissions accounted for O_3 differences of the order of 10 %, both at surface and over the planetary boundary layer (PBL).

1 Introduction

Vegetation fires release large amount of aerosols and trace gases, in particular, carbon dioxide (CO_2), carbon monoxide (CO), nitrogen oxides (NO_x), ammonia (NH_3), particulate matter (PM) and volatile organic compounds (VOC) into the atmosphere (Andreae and Merlet, 2001). The fire-originated masses can significantly alter the chemical state of the lower troposphere. Photochemical O_3 production takes place in very young smoke plumes, within a few tens of minutes after the release (Goode et al., 2000; Jost et al., 2003; Yokelson et al., 2003). It can also be detected several days later in the downwind plumes (Wotawa and Trainer, 2000; Forster et al., 2001; Real et al., 2007).

ACPD
12, 3467–3507, 2012

The transformations of the primary tracers in young plumes are significant, as they substantially alter the plume composition before the smoke is diluted to the regional haze (Jost et al., 2003). The net O_3 production rate in these plumes has been estimated of the order of 20–25 ppb h^{-1} (Jost et al., 2003; Trentmann et al., 2003). Far downwind of large fire events the O_3 concentrations increase; e.g. up to 30 ppb have been reported (McKeen, 2002; Fu et al., 2011; Kogan et al., 2011). Studies in the USA suggest that intense wild-fire periods can significantly increase the frequency of O_3 standards exceedances (Jaffe et al., 2008; Pfister et al., 2008). Furthermore, these pollution events may become more intense and frequent as the climate warms up (Westerling et al., 2006; Jaffe et al., 2008; Carvalho et al., 2011).

The identification of the O_3 episodes related to biomass burning events and their likely source is mainly achieved by ground-based, aircraft, satellite observations, and trajectory calculations (Chung, 1984; Cheng et al., 1998; Damoah et al., 2004; Pfister et al., 2008; Bytnerowicz et al., 2010; Oltmans et al., 2010). The quantification of the fire effects on photochemical oxidants on regional scale is performed with photochemical trajectory models (Ladstätter-Weißenmayer et al., 2005; Real et al., 2007) and chemical transport models (Marufu et al., 2000; Phadnis and Carmichael, 2000; McKeen, 2002; Pfister et al., 2008; Fu et al., 2011; Huang et al., 2011). Despite the enhanced photochemistry that characterizes the fire events, comprehensive model estimates exist mainly for the transport process. Most of these studies have been performed for America and only a few examine the sensitivity of O_3 simulations on fire emission inventories with different spatial and temporal variability (Fu et al., 2011; Huang et al., 2011) and fire emissions characteristics such as NO_x/CO emission ratio and inclusion of VOC (McKeen et al., 2002). Over Europe, most studies investigate the physicochemical properties of aerosols (e.g. Hodzic et al., 2006; Saarikoski et al., 2007; Miranda et al., 2009; Sofiev et al., 2009; Ulevicious et al., 2010) and only a few of them focus on O_3 simulations (Carvalho et al., 2011; Girgždienė and Byčenkienė, 2011).

ACPD
12, 3467–3507, 2012

This study aims to contribute in our wider understanding of O_3 during a wild-land fire event. In particular, the objective of this paper is to investigate the interaction of anthropogenic and natural emission sources during a biomass burning event and their effect on the plume's chemical evolution. We quantify the impact of fire emissions characteristics, such as injection height, magnitude and chemical composition in the whole-PBL and near the surface O_3 production. We demonstrate how a biomass burning event can alter the O_3-NO_x-VOC sensitivity and how this effect depends on the burning material and its chemical properties. Furthermore, the impact of the biogenic emissions in this complex environment is investigated.

The case study is the widespread wild-land fires over Western Russia during spring of 2006. This biomass smoke episode was exceptionally long, lasting about 12 days (24 April and 10 May 2006) (Saarikoski et al., 2007; Stohl et al., 2007; Treffeisen et al., 2007) and caused high O_3 concentrations in Northern and Central Europe. For the numerical simulations, the MM5/CAMx modeling system is used. The fire emissions were generated by the FMI Fire Assimilation System (FAS) based on MODIS Fire Radiative Power (FRP) product (Sofiev et al., 2009). Biogenic emissions include volatile organic compounds (BVOC) from forests, shrubs and crops, as well as NO emissions from agricultural areas. These are estimated with the global Model of Emissions of Gases and Aerosols from Nature (MEGAN) (Guenther et al., 2006). The study complements the previous modeling studies, which assessed the impact of biomass burning on aerosols during this fire event (Saarikoski et al., 2007; Stohl et al., 2007).

2 Methodology, modeling tool, and input data

The collection of the model simulations of this study includes the reference and a series of sensitivity runs using different emission setups. The emission data for the reference run includes anthropogenic, biogenic and biomass burning emissions. The impact of the biomass burning emissions is assessed via the no-fire scenario (NoFIRES). The impact of biogenic emissions under fire conditions is assessed via the no-biogenic

ACPD
12, 3467–3507, 2012

scenario (NoBIOG). The NoBIOG + NoFIRES scenario was also considered for the sake of completeness. Additional sensitivity simulations focus on the fire emission parameters, such as injection height, emissions magnitude and burning material and are compared to the reference run.

2.1 Atmospheric chemistry-transport models

CAMx (Environ, 2004) is an Eulerian photochemical dispersion model that simulates the dispersion, chemical reaction, and removal of pollutants for both gaseous and particulate phase, in the troposphere by solving the pollutant continuity equation. CAMx model was applied in LATLON projection. The study area covers Europe (32.9°–71.9° N; −12.2° W–41.8° E) with spatial resolution 0.4° × 0.2° (135 × 195 cells). The initial and boundary conditions are temporally and spatially constant concentrations based on climatological data. In this study, we focus on the gas phase chemistry results simulated with CB-IV chemical mechanism (Gery et al., 1989). The mechanism includes an explicit oxidation mechanism for isoprene, while the terpenes are examined through the chemistry of olefins (OLE), aldehydes (ALD) and parafins (PAR) carbon groups. The TUV radiative transfer and photolysis model (Madronich, 1993, 2000) is used as a CAMx pre-processor to provide the model with a multi-dimensional lookup table of photolytic rates by surface albedo, altitude, zenith angle, haze turbidity, and total O_3 column derived from OMI measurements for each day of the simulation period. Photolysis rates are further adjusted for the presence of clouds using the approach developed for the Regional Acid Deposition Model (Chang et al., 1987).

The meteorological input data are provided by the PSU/NCAR MM5 meteorology non-hydrostatic model (Grell at al., 1994), Version 3-6-1. The model is applied in Lambert Conformal Space projection with a spatial resolution of 30 km × 30 km (279 × 178 cells). In the vertical, 22 non-uniform vertical σ-layers are used extending up to 14 km (100 hPa). The resolution, up to the first 3 km, was designated in order to better simulate the effect of fire emissions; the lowest σ-level (mid-point) is at about

ACPD
12, 3467–3507, 2012

14 m above ground level while nine vertical levels exist up to 3 km (every 100 m up to 0.5 km, every 500 m up to 3 km). CAMx follows the same vertical resolution.

The initial and lateral boundary conditions are provided by the National Centre for Atmospheric Prediction (NCEP) Final Analyses (FNL) data ($1^\circ \times 1^\circ$), every 6 h, and the 25-category USGS land-use classification scheme is adopted, in order to provide land-cover data for the model domain. For the present study, the applied physics parameterizations are: the Medium-Range Forecast (MRF) PBL scheme (Hong and Pan, 1996), the Grell cumulus scheme (Grell, 1993), the Schultz micro-physics scheme (Schultz, 1995), the Cloud-Radiation scheme (Dudhia, 1989), and the Noah Land Surface Model (Chen and Dudhia, 2001). All the meteorological data, necessary for CAMx simulations, were regridded on the $0.4^\circ \times 0.2^\circ$ CAMx grid by applying the mm5camxv4.3 pre-processor.

EMEP anthropogenic "expert" emissions of NO_x, SO_x, non-methane VOC (NMVOC), CO, NH_3, and PM have been used covering 11 SNAP categories plus emissions from ships and volcanoes (SO_x), for the reference year 2004. The speciation of the anthropogenic NMVOC for each SNAP category is based on Passant (2002). The simulations cover the period from 25 April to 9 May 2006 with two days spin-up.

2.2 Biogenic emissions

Biogenic emissions have been estimated for each hour of the examined period and implemented in the model setup. The net emission rate of each trace gas compound ($mg\,m^{-2}\,h^{-1}$) was calculated from landcover and weather data, by applying the MEGAN algorithm. In particular, monthly average Leaf Area Index (LAI) and standard emission factors were taken from the National Center of Atmospheric Research (NCAR) at a base resolution of 30 s × 30 s and with reference year 2003 and 2000, respectively. In this study, the standard emission factors are weighted averages of five plant functional types (broadleaf trees, needle trees, crops, shrubs and grass). Prior to their use, the landcover data were regridded on the required spatial resolution, $0.4^\circ \times 0.2^\circ$. The necessary meteorological data, namely the fields of hourly surface temperature

ACPD
12, 3467–3507, 2012

and solar radiation were provided by MM5 simulations and regridded with mm5camx pre-processor. Thereafter, the emissions of isoprene, terpenes, biogenic oxygenated volatile organic compounds (BOVOC) and NO emissions have been calculated. The impact of fires on isoprene and monoterpenes emissions as these have been calculated by Alessio et al. (2004) has not been considered, in this study.

In Fig. 1, the spatial distribution of the daily BVOC emission rates over Europe for the period 2 to 7 May is presented. The highest BVOC emissions are found over the Iberian Peninsula, Morocco, Tunisia, parts of Italy, France, Austria, Western Turkey and Russia, which is in agreement with the recent studies (e.g. Simpson et al., 1999; Curci et al., 2009). In particular, Spain appears as the major hot spot for BVOC emissions, displaying daily values up to 10 mg m^{-2} day^{-1}. Despite its high emission potential, relatively low emissions are observed in Scandinavia (0.5–2 mg m^{-2} day^{-1}), mainly due to low solar radiation and surface temperature. Over Central Europe, UK and Western Russia, BVOC emissions reach up to 4.5 mg m^{-2} day^{-1}, depending on the prevailing atmospheric conditions.

During the simulated period, the total BVOC and NO emissions released over the modeling domain are estimated equal to 170.2 and 2.4 kt, respectively. Among the BVOC, the larger fraction 43.4 % is for isoprene, 17.4 % for terpenes (analyzed in 39 % for a-pinene, 17 % for b-pinene, 10 % ocimene, 12 % limonene, 11 % 3-carene and about 5 % for myrcene and sabinene) and 39.1 % for BOVOC (99 % methanol and 1 % methyl butenol). The daily average BVOC and NO emissions are estimated equal to 11.35 ± 0.99 kt (17.35 ± 1.54 g m^{-2}) and 0.16 ± 0.02 kt (0.24 ± 0.03 g m^{-2}), respectively. It is difficult to compare directly our results with those of other studies, because different simulation periods were used. However, the calculated values of BVOC emissions in several hot spots in Europe are of the same magnitude with those from previous studies (Curci et al., 2009; Poupkou et al., 2010). The quite lower terpenes, relative to isoprene emissions, estimated in this study, are mainly due to higher uncertainties related to terpenes emissions estimates that may result from different (a) model approaches, (b) emission factors, (c) land use data, (d) biomass density or a combination of all

ACPD
12, 3467–3507, 2012

these factors (Arneth et al., 2008; Steinbrecher et al., 2009). Another possible reason could be the difference in temperature and solar radiation used for the calculations as our simulation period was April–May.

In order to evaluate MEGAN estimations over the area, during the period of study, the simulated isoprene concentrations are compared to observations from stations of the EMEP network. Isoprene has been chosen for comparison since its chemistry is described explicitly by CB-IV mechanism. During the simulation period, observations from nine stations are available with only 2 % of valid data. In Fig. 2, isoprene time series are presented at six stations; two in France (FR0015 and FR0008), one in Finland (FI0009), one in Slovakia (SK0006), one in Switzerland (CH0005), and one in Czech Republic (CZ0003). Out of these, only CH0005 provide sufficient amount of observations to represent the diurnal variations of the concentrations. The comparison showed that the diurnal cycle is reproduced with temporal correlation coefficient 0.366. The mean absolute levels are within a factor of 2 at Finnish, Swiss, and Slovakian sites but underestimated at the French station FR0008R.

2.3 Fire emissions

Gaseous and PM emission fluxes from biomass burning have been considered. The daily patterns of PM emission fluxes, generated by the FMI FAS system (Sofiev et al., 2009), are based on MODIS FRP product and the recalibrated methodology of Ichoku and Kaufman (2005). A normalization function is used for the hourly variation of the fire intensity. The chemical and size distribution of total PM fire emissions are based on literature review (Andreae et al., 1998; Andreae and Merlet, 2001). The patterns of all the other emission fluxes follow the PM ones and are based on scaling factors relative to total PM, considering grass as the burning material (Andreae and Merlet, 2001). The gaseous emission flux of CO, NO_x (as NO), SO_2, NH_3 and speciated NMVOC emissions is estimated 8.9 times larger than the particulate mass flux and its composition is 88.3 % of CO, 4.6 % of NMVOC, 5.3 % of NO_x, 1.4 % of NH_3, and 0.5 % of SO_2 (mass fractions). The speciation of NMVOC is according to Andreae

ACPD
12, 3467–3507, 2012

and Merlet (2001). In Fig. 3, the daily NO_x emissions, originated from fires during the period 2 to 7 May, are presented. The vertical distribution of fire emissions is spatially constant up to 1000 m; 20 % uniformly distributed up to 100 m (two vertical layers), 30 % uniformly distributed between 100 and 500 m (three vertical layers), and 50 % uniformly distributed up to 1000 m (two vertical layers) (Sofiev et al., 2009).

For the examined period, the daily average NO_x and NMVOC fire emissions injected in the modeling domain is 66.6 ± 36.9 and 58.0 ± 32.2 kt, respectively. In Fig. 4, the daily NO_x and NMVOC emissions from biomass burning are compared with the other emission sources modeled in this study over Europe. The strength of fire emissions during the episode exceeds combined European anthropogenic and biogenic emissions for NO_x, PM, and NMVOC. The rates become comparable only during the last days of the episode.

3 Results

3.1 Episode analysis – comparison with O_3 observations

During this wild-land fire event, unusually high temperatures (close to or above 20 °C) over most of Eastern Europe and Western Russia prevailed. A long-lasting anticyclonic system over Western Russia favored fairly low wind speeds limiting the dilution of anthropogenic pollutants over Central and Eastern Europe. At the beginning of May (2–8 May), the resulting pollution cloud was blown towards the west leading to strong deterioration of air quality in most of Central and Northern Europe up to Iceland (Stohl et al., 2007). Before that, severe degradation of air quality was registered in Finland where the smoke was transported already in April (Saarikoski et al., 2007).

In Fig. 5, the observed daily maximum mean hourly concentrations at 117 rural background monitoring EMEP stations (http://www.emep.int) are shown for the period 2–7 May. In the same plots, the predicted daily maximum mean hourly O_3 concentration is presented as color shades. The calculated maximum concentrations range between

ACPD
12, 3467–3507, 2012

45 and 55 ppb over the major part of Europe, while higher concentrations 60–70 ppb are predicted at some stations over Southern Europe and Black Sea. Regarding the elevated observed concentrations over Northern Europe (75–85 ppb), the model is not able to reproduce them before 2 May. Higher O_3 concentrations are simulated after 3 May, but only on 5, 6, 7 and 8 May two rich-in O_3 plumes are discerned; one over Western Russia moving westwards (70–90 ppb) and the second one extending over Eastern Europe up to North and Baltic Sea (85–90 ppb). The simulated plumes evidently travel beyond the actual developments; however the bulk of high concentrations is not covered by the network (sea, sparse sites, etc.).

The performance of the model is assessed using average and peak statistical metrics. The statistical analysis includes the calculation of the predicted and observed average, the mean normalized bias (MNB), the mean normalized error (MNE), the mean fractional bias (MFB), the mean fractional error (MFE), the root mean square error (RMSE), and the time-paired and time-unpaired peak normalized bias and normalized error. The estimation of the statistical metrics for the whole period, over all stations and over the stations of Central and Northern Europe is presented in Table 1. The definition, according to US EPA, of the metrics is presented in the Appendix A.

Though the model predictions successfully follow the observations' spatial distribution, an underestimation is visible for both average and peak predictions (Table 1). The MNB during the whole simulation period and over all stations is −2.70 %. The agreement is better over Central Europe (MNB = −0.13 %) than over Northern Europe (MNB = −5.34 %). The higher bias over Northern Europe is partly attributed to the model weakness to retain non-zero O_3 concentrations during the night hours, in a number of stations. The day-by-day statistical processing reveals that the MNB and MNE over all stations vary between −15.49 % and 17.97 % and between 30.21 % and 59.02 %, respectively. In some exceptional cases there is a positive bias that comes from a few data points (low observed values) that dominate the metric. For that purpose the MFB is also used where normalization is achieved not by the observed quantity alone, but by both observed and modeled quantities. The day-by-day variation

ACPD
12, 3467–3507, 2012

of the MFB and MFE for all the stations and for the stations of Central and Northern Europe are presented in Fig. 6a. During the first days of the simulation period (25 April–1 May), the model underpredicts the observed concentrations over Northern Europe and specifically over Finland. However, the model predicts higher concentrations after 2 May (see also the next section). Over Northern Europe, these high model predictions decrease the biases towards the end of the simulation period. Over Central Europe the underestimation is still evident even during the days of maximum photochemical activity (4–8 May), probably due to late O_3 plumes arrival to several stations (Fig. 5). The better correlation during the second period, 2–9 May, ($r = 0.49$) compared to the first one, 25 April–1 May, ($r = 0.28$) is also observed in the scatter plots of the mean hourly predicted versus observed O_3 concentrations (Fig. 7).

In contrast to the average metrics, the agreement of the peak metrics is better over the stations of Northern than Central Europe; the unpaired normalized bias is −15.12 % and −20.73 %, respectively. The higher bias at Central Europe is associated with deviations at a number of stations covered by the core of the enhanced O_3 plume (e.g. Poland, Austria, Slovakia). The day-by-day statistical processing over all stations reveals that the unpaired peak normalized bias ranges between −8.90 % and −21.71 % while over Central and Northern Europe it ranges between −3.90 % and −29.59 %, and −6.08 % and −22.88 %, respectively (Fig. 6b). The peak timing bias (difference between the predicted and observed peak hour) over all stations does not exceed ±2 h over 1 day for the whole simulation period (Fig. 6b).

A comprehensive analysis of the model bias would ideally relate the sensitivity of model predictions to various aspects, such as the chemical mechanism, grid resolution, boundary conditions, and emissions. However, this is beyond the scope of this study. Our principal objective is to investigate the model sensitivity to the interaction of natural and anthropogenic emission sources.

ACPD
12, 3467–3507, 2012

3.2 Impact of fire emissions

The interpretation of the influence of the biomass burning emissions on the model results is discussed below through the O_3-NO_x-VOC sensitivity. In general, large NO_x sources (e.g. urban areas or polluted remote areas) are characterized by low VOC/NO_x ratios and correspond to the VOC-sensitive regime. In the VOC-sensitive regime, O_3 increases with increasing VOC and decreases with increasing NO_x (Sillman, 1999). On the contrary, remote areas are usually characterized by low ambient NO_x and high BVOC emission levels, thus by fairly high VOC/NO_x ratios and correspond to the NO_x-sensitive regime. In the NO_x-sensitive regime, O_3 increases with increasing NO_x and shows relatively little change in response to increased VOC. Beekmann and Vautard (2010) discussed the spatial distribution of the NO_x-VOC sensitive regimes over Europe and their temporal variability. They concluded that the northwestern Europe lies in the VOC-sensitive regime while Mediterranean and Eastern Europe are in the NO_x-sensitive regime. Below, it is shown that the biomass burning can alter the O_3 sensitivity over the wider area that is influenced by the dispersion of fire plumes (Eastern Europe and Western Russia).

The critical role of the biomass burning emissions was demonstrated through the NoFIRES scenario. In Fig. 8, the maximum influence of fire emissions on mean hourly surface O_3 concentrations (differences between the reference and the NoFIRES scenarios) is presented for each day of the period 2–7 May. It is seen that the fire emissions determine the spatial distribution of surface O_3 over large parts of Europe and contribute to its maximum values over Northern and Eastern Europe up to 40–45 ppb (~80 %). However, in the close vicinity of the fire spots lower O_3 concentrations (up to 40 ppb) are predicted. In contrast to expected usual VOC and NO_x concentrations, the fire event releases very large amount of NO_x, thus, the low VOC/NO_x concentration ratios prevail over the area of interest. In Fig. 9, the spatial distribution of the simulated VOC/NO_x ratios is presented for the period 2–7 May, at 12:00 UTC. Until 3 May, the ratios range between 1 and 3 ppbC ppb^{-1}, lower than those characterizing Central

ACPD
12, 3467–3507, 2012

Europe (4–15 ppbC ppb^{-1}). Under these conditions, the O_3 production over the area of interest is rather characterized as VOC-sensitive and is mainly controlled by the VOC-OH oxidation reactions. These findings are in agreement with the studies of Mason et al. (2001) and Trentmann et al. (2003), who also pointed out the VOC-sensitivity of the O_3 production in biomass burning plumes. Under normal conditions over Scandinavia, relatively high BVOC emissions and almost negligible impact of fire NO_x emissions usually result in high ratios (~55 ppbC ppb^{-1}).

The chemistry leading to O_3 production is initiated by reactions of hydroxyl (OH) radicals with CO and VOC. These reactions produce peroxy radicals (HO_2, RO_2) which then convert NO to NO_2 leading to O_3 formation. In Fig. 10, the integrated hourly oxidation rates of total, anthropogenic and natural, VOC-OH reactions (including C_1 components, CO and CH_4) are presented for 2–7 May, at 12:00 UTC. During all days, the fire spots exhibit the highest VOC-OH oxidation rates, up to 30 ppb h^{-1} (during 25–27 April up to 50 ppb h^{-1}, not shown). A significant fraction of the VOC-OH oxidation rate (30 %) is due to the abundance of the CO fire emissions. Accordingly, O_3 production rates (determined as the rate at which peroxy radicals react with NO) reach up to 60 ppb h^{-1} and at the same time it is highly depleted, due to its reaction with the emitted NO, leading to low surface O_3 concentrations, up to 30 ppb (Fig. 5), as was also pointed out by Trentmann et al. (2003).

The analysis of model predictions reveal that prerequisite for the O_3 production excess is the combined effect of favorable meteorological conditions, increased BVOC and decreased fire-originated NO_x. The oxidation capacity of the atmosphere is not adequate to produce O_3 excess before 3 May. After that date, the increase of water vapor over Central and Northern Europe and Western Russia contributes to higher "new" OH radical concentrations initiated by O_3 photolysis (Fig. 10). The oxidation capacity over the eastern part of the domain (Eastern Europe and Western Russia) during 3–5 May is further enhanced due to the increased biogenic activity (Fig. 1). In particular, the BVOC oxidation produces secondary carbonyl species, whose photolysis provides additional radicals. Eventually, the admixture of reactive BVOC emissions combined

ACPD
12, 3467–3507, 2012

with the decrease of the fire NO_x emissions after 3 May (Figs. 3, 4) favors the O_3 increase in the VOC-sensitive environment.

As the episode evolves, 4–5 May, the VOC/NO_x ratios over Western Russia increase, and ends with O_3 increases up to 40 ppb. During the next days, 6 and 7 May, the O_3 plume is transported westwards (Fig. 12) and is enhanced over Baltic Sea and Helsinki (Fig. 5). Over Germany and Denmark up to the North Sea, a second plume is extended through a SSE-NNW axis due to the accumulation of "new" OH radicals, produced under the favorable conditions of increased radiation and water vapor (Fig. 10). The O_3 accumulation over Baltic and North Sea is due to lower deposition velocities. The decrease of fire intensity during the last days of the episode, 8–9 May, further increases the VOC/NO_x ratios up to 25 ppbC ppb^{-1} (not shown) over the area shifting the chemistry towards the NO_x-sensitive regime and smoothes out the O_3 gradients. It is interesting that downwind of the fire plume, the less reactive CO emissions, compared to VOC, arrive intact, and contribute to the VOC-OH oxidation rates by 40–50 %. Omitting CO from the fire gaseous mixture results in O_3 decreases by 20–25 % while with no VOC the impact is lower, 5–10 % (not shown).

3.3 Impact of biogenic emissions

In order to assess the impact of biogenic activity during this wild-land-fire event, a series of no biogenic emissions scenarios (NoBIOG) has been performed with complete or partial suppression of the BVOC emissions. The maximum influence on mean hourly surface O_3 concentrations during the whole simulation period is presented in Fig. 11a (complete elimination of all BVOC). As one can see, the biogenic activity increases O_3 values over the continent by an average of 0.5 ppb. However, the impact on the maximum hourly surface O_3 concentrations over specific areas is up to 8 ppb and is observed during the afternoon hours.

Additional simulations revealed the BVOC category which mostly contributes in surface O_3 increases. These scenarios consider the anthropogenic and biomass burning emissions as in the reference run, but with one of the BVOC categories: (a) only

ACPD
12, 3467–3507, 2012

isoprene, (b) only terpenes and, (c) only BOVOC emissions. In Fig. 11b–d, the maximum changes of the mean hourly surface O_3 predictions in the reference run in relation to the NoBIOG runs (partial elimination) are presented. Isoprene is the major contributor to the O_3 increases, by 80 % (up to 6 ppb). Terpenes and BOVOC emissions have lower contribution, 0.5–1 ppb, likely because of lower emissions for the terpenes case and the low reaction rates for the BOVOC category. Even though the emission load of isoprene and BOVOC categories is comparable, the methanol's (99 % of BOVOC) low oxidation rate by OH radical (1600 ppm min^{-1} compared to isoprene's 147 600 ppm min^{-1}) results in low O_3 productivity. Due to the low BOVOC reactivity, O_3 increases are evident only over areas with maximum BOVOC emissions (>0.5 mg m^{-2} day^{-1}, Fig. 11d). On the contrary, the most reactive compounds, isoprene and terpenes, interact substantially with fire emissions and exhibit additional areas of influence.

During the days of low biogenic activity (until 1 May), the BVOC emissions result in the O_3 increase, up to 1 ppb over Eastern Europe, Western Russia and Scandinavia – for the areas with elevated fire NO_x emissions (not shown). The impact is getting higher after 3 May, under the favorable conditions for the VOC chemistry discussed in the previous section, and it is maximized between 4 and 5 May, reaching up to 8 ppb (Fig. 12). During these days, isoprene contributes to the VOC-OH oxidation rates, up to 30 % over Western Russia and 5 % over Eastern Europe (when CO and CH_4 are not considered in the VOC mixture). On 6 and 7 May, the impact of BVOC emissions is emphasized on the rich-in O_3 plumes. Finally, during 8 May, even though BVOC emissions over Western Russia are comparable with the emissions during the previous days (2.5–3 mg m^{-2} day^{-1}, not shown), their impact on surface O_3 does not exceed 1 ppb. Under low fires activity (Fig. 3) and low NO_x concentrations, the peroxy radicals, produced by VOC-OH oxidation, are removed from the system through radical-radical reactions, rather than participating in chain reactions converting NO to NO_2.

Over the rest of Europe, the mean hourly O_3 increases do not exceed 2 ppb (Fig. 12). The increase near UK, on 3 and 4 May, is attributed mainly to the interaction of BVOC

ACPD
12, 3467–3507, 2012

emissions and ports activity while at Norway, on 6 May, the necessary oxidation fuel is provided by a fire spot. Despite the fact that over the southern Europe, biogenic activity and isoprene-OH oxidation rates (Fig. 13), exhibit the highest values in Europe, the lack of essential NO_x for efficient O_3 production leads in relatively small O_3 increases. The same result (e.g. for Spain) has been also discussed by Curci et al. (2009). The negative O_3 differences at the southeastern edge of the domain (Fig. 12) are associated with ozonolysis of isoprene and terpenes and mainly reflect the absence of anthropogenic NO_x emissions.

It is worth mentioning that in the absence of fire emissions, the normally expected NO_x-limited environment over Eastern Europe and Western Russia determines the role of biogenic emissions. The runs with and without biogenic emissions under no-fire conditions (NoFIRES and NoBIOG + NoFIRES) revealed negligible or even negative O_3 differences (−1 ppb) over Eastern Europe and Western Russia due to BVOC ozonolysis (not shown). During the days of maximum photochemical activity and in the absence of fires, isoprene contributes to the VOC-OH oxidation rates, up to 50 % over Western Russia and 10 % over Eastern Europe (when CO and CH_4 are not considered in the VOC mixture). These fractions are higher compared to the fire conditions case, as the presence of fire VOC emissions depresses OH levels, thereby reduces the reactivity of BVOC emissions. Nevertheless, the absence of fire NO_x emissions eliminates the O_3 forming potential of BVOC emissions. Over the rest of Europe, the impact of biogenic activity remains almost the same, as it is not influenced by the presence of the wild-land fire event.

3.4 Sensitivity to parameters of the fire emissions

In this section, we present results from sensitivity tests regarding key parameters of fire emissions namely the injection height, the chemical composition and the magnitude on model predictions.

According to Sofiev et al. (2009), the fire event investigated in this study was largely a dry grass fire. The burning material mainly consisted of previous-year grass remnants,

ACPD
12, 3467–3507, 2012

which were dried up by the beginning of the fires. Literature review concludes that Eastern Europe and Russia are the greatest contributors to agricultural fires injecting the fires smoke mostly within the mixing layer (Labonne et al., 2007; Sofiev et al., 2009; Amiridis et al., 2010). However, some authors claim that emissions from forest and mixed areas are also substantial (e.g. Labonne et al., 2007), injecting releases above the PBL. In order to examine the sensitivity of the model results on fire emission injection height, two additional scenarios are considered. In the first one (F1), the daily maximum injection height is set spatially and temporally constant (as in the reference run) and is determined by the calculated daily maximum PBL height over the burnt area (3–4 May 2.3 ± 0.2 km, 5 May 2.4 ± 0.2 km, 6 May 2.2 ± 0.3 km, 7 May 1.8 ± 0.4 km, 8 May 1.6 ± 0.3 km). According to F1, the 50 % of fire emissions load is distributed up to 500 m, as in the reference run while the remaining 50 % is distributed uniformly up to the PBL height. The second scenario (F2) assesses the impact of possible crown fires. In particular, the assumptions of the KAS05.D2 scenario adopted by Leung et al. (2007) are considered. According to this scenario, the majority of fires are crown fires, thus a large fraction (60 %) of the emissions is injected above the top of the PBL up to 5 km. The rest (40 %) of the fire emissions represents emissions from surface fuels and is uniformly distributed up to a representative average PBL height over the burnt area (2.5 km).

The differences between F1 and the reference run reflect differences in the distribution of emissions between 500 m and the maximum top of the PBL height. In the vicinity of the fires, F1 scenario predicts higher surface O_3 concentrations ranging between 3 and 10 %. The release of fire emissions up to higher altitudes favors the O_3 enhancement within the PBL (up to 7 %) which under favorable conditions is mixed downward increasing surface concentrations. The highest differences (8 ppb) are predicted during the days of maximum photochemical activity. The differences are much more pronounced for the F2 scenario. The lower NO_x emissions released at surface and inside the PBL, in relation to the reference run, enhance O_3 production within the PBL up to 10 %. At surface and in regions where biomass burning emissions exist, the

ACPD
12, 3467–3507, 2012

concentrations are higher up to 25 % (22 ppb). However, in the rich-in O_3 plume, along the SSE-NNW axis, the maximum surface values decrease by 5–8 % (up to 8 ppb) due to lower NO_x concentrations.

Regarding the composition of the gaseous mixture released by the fires, it is proven critical for the O_3-NO_x-VOC sensitivity and the episode evolution. Studies demonstrate that the NO_x/CO emission ratio from the fires is highly uncertain and variable (Mason et al., 2001; McKeen et al., 2002). In this study, two different molar NO_x/CO ratios are examined, both retrieved from Andrea and Merlet (2001); the ratio of 0.06 has been used in the reference run which reflects the properties of grassland as burning material, while a lower ratio, 0.025, reflects the properties of agricultural residues (89.1 % of CO, 6.8 % of NMVOC, 2.4 % of NO_x, 1.3 % of NH_3, and 0.4 % of SO_2 mass fractions). In case of the low-NOX fractionation, the VOC/NO_x ratios over Eastern Europe and Western Russia become quite high (~50 ppbC ppb^{-1}), compared to the reference run, mainly due to lower NO_x emissions but also higher (almost by a factor of 1.5) VOC emissions. The significant reduction of the bias (Table 1), is mainly attributed to the higher, almost by a factor of 2, VOC-OH oxidation and O_3 production rates at the fire spots, compared to the reference run. In addition, the prevention of O_3 scavenging in their vicinity yields higher surface O_3 concentrations by a factor of 2 (up to 150 ppb), during the whole simulation period. However, over Scandinavia the predictions overestimate the observations by up to 50 %. In the areas characterized by rich-in O_3 plumes, the low ratio yields higher O_3 predictions (up to 17 %), while the predictions over Central Europe change only slightly. For both cases, the main nitrogen reservoir species downwind of the fires are nitric acid (HNO_3) and peroxyacetyl nitrate (PAN), accounting for about 75 and 25 %, respectively, in the case of high NO_x/CO ratio and 30–50 and 40 % in the case of the low one. The great sensitivity of model results on the fire mixture composition indicates the need of regional fire emission databases over Europe, similar to those presented for Portugal by Alves et al. (2011).

The predictions are less sensitive on the magnitude of fire emissions. According to Ichoku and Kaufman (2005), the methodology to convert the FRP to PM emission

ACPD
12, 3467–3507, 2012

fluxes, used in this study, involves uncertainties and a possible overestimation of PM emission fluxes by 50 %. In order to deal with these uncertainties, a simulation with a 20 % cut-off of all fire emissions has been conducted. This reduction invokes a decrease of the maximum hourly surface O_3 concentrations inside the rich-in O_3 plumes (Eastern and Northern Europe, Western Russia) by 5–10 %. Under these conditions, the impact of biogenic activity decreases, in relation to the reference run, up to 3 ppb. In contrast, close to the fire spots where O_3 titration by NO prevails, the maximum hourly surface O_3 concentrations increase up to 20 %.

4 Conclusions

In the frame of this modeling study, the interactions of anthropogenic, natural, and biomass burning emissions are investigated using an O_3 episode over Europe caused by wild-land fires over Western Russia. Biomass burning is shown to be critical for the episode contributing up to 45 ppb to maximum hourly surface O_3.

The fire event also determined the sensitivity of the O_3 chemistry on its precursors. CO and VOC fire emissions affect O_3 maximum concentrations by 20–25 % and 5–10 %, respectively. Biomass burning is found to be a major source of reactive nitrogen species. Nitric acid and peroxyacetyl nitrate are the major contributors, accounting for about 75 % and 25 % of the total nitrogen reservoir species. However, close to the fires O_3 is highly depleted due to its reaction with the emitted NO. Downwind of the fires, the areas mostly affected are designated by the combination of several factors, such as high water vapor, relatively high biogenic emissions, abundance of NO_x and favorable wind flow.

The impact of chemical composition of the fire emissions is examined via two sensitivity simulations, one with high (0.06) and one with low (0.025) NO_x/CO molar ratios. In case of the high fire NO_x/CO ratio, the area (Eastern Europe – Western Russia) is characterized by low VOC/NO_x ratios and VOC-sensitive O_3 production. Fire spots exhibit O_3 production rates up to 60 ppb h^{-1}. In case of the low fire NO_x/CO molar ratio,

ACPD
12, 3467–3507, 2012

the area is characterized by lower NO_x emissions and NO_x-sensitive O_3 production. Over Western Russia and Scandinavia, the surface O_3 predictions almost double, due to higher O_3 production rates at the fire spots and lower O_3 scavenging in their vicinity leading to a model-observation positive bias at (few) observation sites in these areas.

Changing the vertical distribution of fire emissions, inside the PBL, results in O_3 differences, at surface and within the PBL, of the order of 10 %.

During the fire episode, the effect of BVOC emissions on surface O_3 concentrations in the afternoon is significant, up to 8 ppb, and isoprene is the major contributor (80 %). The interaction of BVOC and fire NO_x emissions is critical. Along the vertical, the impact of BVOC emissions is evident up to 4.5 km and reaches up to 5 ppb. Under NO_x-limited environment or in the absence of fires, the impact of BVOC emissions is almost negligible.

The comparison with isoprene observations at stations of the EMEP network shows that isoprene estimations, based on MEGAN algorithm, are quite satisfactory preserving in general the observed temporal variation.

Appendix A

A1 Average statistics

N is the product of the number of simulation hours and the number of monitoring locations, C_o is the observed value, C_p is the predicted value.

$$\text{Average Predicted} = \frac{1}{N}\sum_{i=1}^{N} C_{p_i}, \quad \text{Average Observed} = \frac{1}{N}\sum_{i=1}^{N} C_{o_i},$$

$$\text{Mean Normalized Bias} = \frac{100}{N}\sum_{i=1}^{N}\left(\frac{C_{p_i}-C_{o_i}}{C_{o_i}}\right),$$

$$\text{Mean Normalized Error} = \frac{100}{N}\sum_{i=1}^{N}\left|\frac{C_{p_i}-C_{o_i}}{C_{o_i}}\right|,$$

ACPD
12, 3467–3507, 2012

$$\text{Mean Fractional Bias} = \frac{200}{N}\sum_{i=1}^{N}\left(\frac{C_{\mathrm{p}_i}-C_{\mathrm{o}_i}}{C_{\mathrm{p}_i}+C_{\mathrm{o}_i}}\right),$$

$$\text{Mean Fractional Error} = \frac{200}{N}\sum_{i=1}^{N}\left|\frac{C_{\mathrm{p}_i}-C_{\mathrm{o}_i}}{C_{\mathrm{p}_i}+C_{\mathrm{o}_i}}\right|,$$

$$\text{RMSE} = \sqrt{\frac{1}{N}\sum_{i=1}^{N}\left(C_{\mathrm{p}_i}-C_{\mathrm{o}_i}\right)^2}$$

A2 Peak statistics

N is the number of monitoring stations, $C_{\mathrm{o}}(x,t')_{\max}$ and $C_{\mathrm{p}}(x,t)_{\max}$ are the maximum hourly observed and predicted concentrations at a specific monitoring station over a time period, $C_{\mathrm{p}}(x,t')_{\max}$ is the maximum hourly predicted concentration at the same monitoring station at the time of the observed peak.

$$\text{Time-paired peak normalized bias} = \frac{100}{N}\sum_{i=1}^{N}\frac{C_{\mathrm{p}}(x,t')_{\max}-C_{\mathrm{o}}(x,t')_{\max}}{C_{\mathrm{o}}(x,t')_{\max}}$$

$$\text{Time-paired peak normalized error} = \frac{100}{N}\sum_{i=1}^{N}\left|\frac{C_{\mathrm{p}}(x,t')_{\max}-C_{\mathrm{o}}(x,t')_{\max}}{C_{\mathrm{o}}(x,t')_{\max}}\right|$$

$$\text{Time-unpaired peak normalized bias} = \frac{100}{N}\sum_{i=1}^{N}\frac{C_{\mathrm{p}}(x,t)_{\max}-C_{\mathrm{o}}(x,t')_{\max}}{C_{\mathrm{o}}(x,t')_{\max}}$$

$$\text{Time-unpaired peak normalized error} = \frac{100}{N}\sum_{i=1}^{N}\left|\frac{C_{\mathrm{p}}(x,t)_{\max}-C_{\mathrm{o}}(x,t')_{\max}}{C_{\mathrm{o}}(x,t')_{\max}}\right|$$

Acknowledgements. This paper has been part of the actions COST728 and COSTES0602.

References

Alessio, G. A., De Lillis, M., Fanelli, M., Pinelli, P., and Loreto, F.: Direct and indirect impacts of fire on the isoprenoids emission from Mediterranean vegetation, Funct. Ecol., 18, 357–364, 2004.

ACPD
12, 3467–3507, 2012

Alves, C., Vicente, A., Nunes, T., Gonçalves, C., Fernandes, A. P., Mirante, F., Tarelho, L., Sánchez de la Campa, A. M., Querol, X., Caseiro, A., Monteiro, C., Evtyugina, M., and Pio, C.: Summer 2009 wildfires in Portugal: Emission of trace gases and aerosol composition, Atmos. Environ., 45, 641–649, 2011.

Amiridis, V., Giannakaki, E., Balis, D. S., Gerasopoulos, E., Pytharoulis, I., Zanis, P., Kazadzis, S., Melas, D., and Zerefos, C.: Smoke injection heights from agricultural burning in Eastern Europe as seen by CALIPSO, Atmos. Chem. Phys., 10, 11567–11576, doi:10.5194/acp-10-11567-2010, 2010.

Andreae, M. O. and Merlet, P.: Emissions of trace gases and aerosols from biomass burning, Global Biogeochem. Cy., 15, 955–966, 2001.

Andreae, M. O., Andreae, T. W., Annegarn, H., Beer, J., Cachier, H., Le Canut, P., Elbert, W., Maenhaut, W., Salma, I., Wienhold, F. G., and Zenker, T.: Airborne studies of aerosol emissions from savanna fires in southern Africa: 2. Aerosol chemical composition, J. Geophys. Res., 103, 32119–32128, 1998.

Arneth, A., Monson, R. K., Schurgers, G., Niinemets, Ü., and Palmer, P. I.: Why are estimates of global terrestrial isoprene emissions so similar (and why is this not so for monoterpenes)?, Atmos. Chem. Phys., 8, 4605–4620, doi:10.5194/acp-8-4605-2008, 2008.

Beekmann, M. and Vautard, R.: A modelling study of photochemical regimes over Europe: robustness and variability, Atmos. Chem. Phys., 10, 10067–10084, doi:10.5194/acp-10-10067-2010, 2010.

Bytnerowicz, A., Cayan, D., Riggan, P., Schilling, S., Dawson, P., Tyree, M., Wolden, L., Tissell, R., and Preisler, H.: Analysis of the effects of combustion emissions and santa ana winds on ambient ozone during the October 2007 southern California wildfires, Atmos. Environ., 44, 678–687, 2010.

Carvalho, A., Monteiro, A., Flannigan, M., Solman, S., Miranda, A. I., and Borrego, C.: Forest fires in a changing climate and their impacts on air quality, Atmos. Environ., 45, 5545–5553, 2011.

Chang, J. S., Brost, R. A., Isaksen, I. S. A., Madronich, S., Middleton, P., Stockwell, W. R., and Walcek, C. J.: A three-dimensional eulerian acid deposition model: physical concepts and formulation, J. Geophys. Res., 92, 14681–14700, 1987.

Chen, F. and Dudhia, J.: Coupling and advanced land surface-hydrology model with the Penn State-NCAR MM5 modeling system. Part I: Model implementation and sensitivity, Mon. Weather Rev., 129, 569–585, 2001.

ACPD
12, 3467–3507, 2012

Cheng, L., McDonald, K. M., Angle, R. P., and Sandhu, H. S.: Forest fire enhanced photochemical air pollution. A case study, Atmos. Environ., 32, 673–681, 1998.
Chung, Y.-S.: On the forest fires and the analysis of air quality data and total atmospheric ozone, Atmos. Environ., 18, 2153–2157, 1984.
Curci, G., Beekmann, M., Vautard, R., Smiatek, G., Steinbrecher, R., Theloke, J., and Friedrich, R.: Modeling study of the impact of isoprene and terpene biogenic emissions on European ozone levels, Atmos. Environ., 43, 1444–1455, 2009.
Damoah, R., Spichtinger, N., Forster, C., James, P., Mattis, I., Wandinger, U., Beirle, S., Wagner, T., and Stohl, A.: Around the world in 17 days - hemispheric-scale transport of forest fire smoke from Russia in May 2003, Atmos. Chem. Phys., 4, 1311–1321, doi:10.5194/acp-4-1311-2004, 2004.
Dudhia, J.: Numerical study of convection observed during the winter monsoon experiment using a mesoscale two-dimensional model, J. Atmos. Sci., 46, 3077–3107, 1989.
Environ: User's guide to the comprehensive air quality model with extensions (CAMx), version 4.10s, report, ENVIRON Int. Corp., Novato, Calif., 2004.
Forster, C., Wandinger, U., Wotawa, G., James, P., Mattis, I., Althausen, D., Simmonds, P., O'Doherty, S., Jennings, S. G., Kleefeld, C., Schneider, J., Trickl, T., Kreipl, S., Jäger, H., and Stohl, A.: Transport of boreal forest fire emissions from Canada to Europe, J. Geophys. Res., 106, 22887–22906, doi:10.1029/2001jd900115, 2001.
Fu, J. S., Hsu, N. C., Gao, Y., Huang, K., Li, C., Lin, N.-H., and Tsay, S.-C.: A regional chemical transport modeling to identify the influences of biomass burning during 2006 BASE-ASIA, Atmos. Chem. Phys. Discuss., 11, 3071–3115, doi:10.5194/acpd-11-3071-2011, 2011.
Gery, M. W., Whitten, G. Z., Killus, J. P., and Dodge, M. C.: A Photochemical Kinetics Mechanism for Urban and Regional Scale Computer Modeling, J. Geophys. Res., 94, 925–956, 1989.
Girgždienė, R., and Byčenkienė, S.: Utilizing satellite data to highlight high ozone concentration events during fire episodes, in: Use of Satellite and In-situ Data to Improve Sustainability, NATO Science for Peace and Security Series C: Environmental Security, edited by: Kogan, F., Powell, A., and Fedorov, O., Springer Netherlands, 191–198, Part 4, doi:10.1007/978-90-481-9618-0_22, 2011.
Goode, J. G., Yokelson, R. J., Ward, D. E., Susott, R. A., Babbitt, R. E., Davies, M. A., and Hao, W. M.: Measurements of excess O_3, CO_2, CO, CH_4, C_2H_4, C_2H_2, HCN, NO, NH_3, HCOOH, CH_3COOH, HCHO, and CH_3OH in 1997 Alaskan biomass burning plumes by

ACPD
12, 3467–3507, 2012

airborne Fourier transform infrared spectroscopy (AFTIR), J. Geophys. Res., 105, 22147–22166, doi:10.1029/2000jd900287, 2000.
Grell, G. A.: Prognostic evaluation of assumptions used by cumulus parameterizations, Mon. Weather Rev., 121, 764–787, 1993.
Grell, G. A., Dudhia, J., and Stauffer, D.: A description of the fifth-generation Penn state/NCAR mesoscale model (MM5), NCAR technical note, NCAR/TN-398 +STR, National Centre for Atmospheric Sciences, Boulder, CO, 138 pp., 1994.
Guenther, A., Karl, T., Harley, P., Wiedinmyer, C., Palmer, P. I., and Geron, C.: Estimates of global terrestrial isoprene emissions using MEGAN (Model of Emissions of Gases and Aerosols from Nature), Atmos. Chem. Phys., 6, 3181–3210, doi:10.5194/acp-6-3181-2006, 2006.
Hodzic, A., Vautard, R., Chepfer, H., Goloub, P., Menut, L., Chazette, P., Deuzé, J. L., Apituley, A., and Couvert, P.: Evolution of aerosol optical thickness over Europe during the August 2003 heat wave as seen from CHIMERE model simulations and POLDER data, Atmos. Chem. Phys., 6, 1853–1864, doi:10.5194/acp-6-1853-2006, 2006.
Hong, S.-Y. and Pan, H.-L.: Nonlocal Boundary-Layer vertical diffusion in a medium-range forecast model, Mon. Weather Rev., 124, 2322–2339, 1996.
Huang, M., Carmichael, G. R., Spak, S. N., Adhikary, B., Kulkarni, S., Cheng, Y., Wei, C., Tang, Y., D'Allura, A., Wennberg, P. O., Huey, G. L., Dibb, J. E., Jimenez, J. L., Cubison, M. J., Weinheimer, A. J., Kaduwela, A., Cai, C., Wong, M., Bradley Pierce, R., Al-Saadi, J. A., Streets, D. G., and Zhang, Q.: Multi-scale modeling study of the source contributions to near-surface ozone and sulfur oxides levels over California during the ARCTAS-CARB period, Atmos. Chem. Phys., 11, 3173–3194, doi:10.5194/acp-11-3173-2011, 2011.
Ichoku, C. and Kaufman, J. Y.: A Method to Derive Smoke Emission Rates From MODIS Fire Radiative Energy Measurements, IEEE T. Geosci. Remote, 43, 2636–2649, 2005.
Jaffe, D., Chand, D., Hafner, W., Westerling, A., and Spracklen, D.: Influence of fires on O_3 concentrations in the Western U.S, Environ. Sci. Technol., 42, 5885–5891, doi:10.1021/es800084k, 2008.
Jost, C., Trentmann, J., Sprung, D., Andreae, M. O., McQuaid, J. B., and Barjat, H.: Trace gas chemistry in a young biomass burning plume over Namibia: Observations and model simulations, J. Geophys. Res., 108, 8482, doi:10.1029/2002jd002431, 2003.
Kogan, F., Powell, A., Fedorov, O., Girgždienė, R., and Byčenkienė, S.: Utilizing Satellite Data to Highlight High Ozone Concentration Events During Fire Episodes, in: Use of Satellite and

ACPD
12, 3467–3507, 2012

In-Situ Data to Improve Sustainability, NATO Science for Peace and Security Series, Springer Netherlands, 191–198, 2011.
Labonne, M., Breon, F.-M., and Chevallier, F.: Injection height of biomass burning aerosols as seen from a spaceborne lidar, Geophys. Res. Lett., 34, L11806, doi:10.1029/2007GL029311, 2007.
Ladstätter-Weißenmayer, A., Meyer-Arnek, J., Richter, A., Wittrock, F., and Burrows, J. P.: Tropospheric O_3 over Indonesia during biomass burning events measured with GOME (Global Ozone Monitoring Experiment) and compared with trajectory analysis, Atmos. Chem. Phys. Discuss., 5, 3105–3130, doi:10.5194/acpd-5-3105-2005, 2005.
Leung, F.-Y. T., Logan, J. A., Park, R., Hyer, E., Kasischke, E., Streets, D., and Yurganov, L.: Impacts of enhanced biomass burning in the boreal forests in 1998 on tropospheric chemistry and the sensitivity of model results to the injection height of emissions, J. Geophys. Res., 112, D10313, doi:10.1029/2006jd008132, 2007.
Madronich, S.: UV radiation in the natural and perturbed atmosphere, in Environmental Effects of UV (Ultraviolet) Radiation, edited by: Tevini, M., Lewis Publisher, Boca Raton, pp. 17–69, 1993.
Madronich, S.: The Tropospheric Visible Ultra-violet (TUV) model web page. National Center for Atmospheric Research, Boulder, CO, http://acd.ucar.edu/TUV/, 2002.
Marufu, L., Dentener, F., Lelieveld, J., Andreae, M. O., and Helas, G.: Photochemistry of the African troposphere: Influence of biomass-burning emissions, J. Geophys. Res., 105, 14513–14530, doi:10.1029/1999jd901055, 2000.
Mason, S. A., Field, R. J., Yokelson, R. J., Kochivar, M. A., Tinsley, M. R., Ward, D. E., and Hao, W. M.: Complex effects arising in smoke plume simulations due to inclusion of direct emissions of oxygenated organic species from biomass combustion, J. Geophys. Res., 106, 12527–12539, doi:10.1029/2001jd900003, 2001.
McKeen, S. A., Wotawa, G., Parrish, D. D., Holloway, J. S., Buhr, M. P., Hübler, G., Fehsenfeld, F. C., and Meagher, J. F.: Ozone production from Canadian wildfires during June and July of 1995, J. Geophys. Res., 107, 4192, doi:10.1029/2001jd000697, 2002.
Miranda, A. I., Marchi, E., Ferretti, M., and Millán, M. M.: Forest Fires and Air Quality Issues in Southern Europe, in: Developments in Environmental Science, 8, edited by: Bytnerowicz, A., Arbaugh, M., Riebau, A., and Andersen, C., Elsevier B.V. 209–231, 2009.
Oltmans, S. J., Lefohn, A. S., Harris, J. M., Tarasick, D. W., Thompson, A. M., Wernli, H., Johnson, B. J., Novelli, P. C., Montzka, S. A., Ray, J. D., Patrick, L. C., Sweeney, C., Jefferson,

ACPD
12, 3467–3507, 2012

A., Dann, T., Davies, J., Shapiro, M., and Holben, B. N.: Enhanced ozone over western North America from biomass burning in Eurasia during April 2008 as seen in surface and profile observations, Atmos. Environ., 44, 4497–4509, 2010.
Passant, N. R.: Speciation of UK emissions of non-methane volatile organic compounds, AEAT/ENV/R/0545 report, London, UK, 2002.
Pfister, G. G., Wiedinmyer, C., and Emmons, L. K.: Impacts of the fall 2007 California wildfires on surface ozone: Integrating local observations with global model simulations, Geophys. Res. Lett., 35, L19814, doi:10.1029/2008gl034747, 2008.
Phadnis, M. J. and Carmichael, G. R.: Forest fire in the boreal region of China and its impact on the photochemical oxidant cycle of East Asia, Atmos. Environ., 34, 483–498, 2000.
Poupkou, A., Giannaros, T., Markakis, K., Kioutsioukis, I., Curci, G., Melas, D., and Zerefos, C.: A model for European Biogenic Volatile Organic Compound emissions: Software development and first validation, Environ. Modell. Softw., 25, 1845–1856, 2010.
Real, E., Law, K. S., Weinzierl, B., Fiebig, M., Petzold, A., Wild, O., Methven, J., Arnold, S., Stohl, A., Huntrieser, H., Roiger, A., Schlager, H., Stewart, D., Avery, M., Sachse, G., Browell, E., Ferrare, R., and Blake, D.: Processes influencing ozone levels in Alaskan forest fire plumes during long-range transport over the North Atlantic, J. Geophys. Res., 112, D10S41, doi:10.1029/2006JD007576, 2007.
Saarikoski, S., Sillanpää, M., Sofiev, M., Timonen, H., Saarnio, K., Teinilä, K., Karppinen, A., Kukkonen, J., and Hillamo, R.: Chemical composition of aerosols during a major biomass burning episode over northern Europe in spring 2006: experimental and modelling assessments, Atmos. Environ., 41, 3577–3589, 2007.
Schultz, P.: An explicit cloud physics parameterization for operational numerical weather prediction, Mon. Weather Rev., 123, 3331–3343, 1995.
Sillmann, S.: The relation between ozone, NO_x and hydrocarbons in urban and polluted rural environments, Atmos. Environ., 33, 1821–1845, 1999.
Simpson, D., Winiwarter, W., Borjesson, G., Cinderby, S., Ferreiro, A., Guenther, A., Hewitt, C. N., Janson, R., Khalil, M. A. K., Owen, S., Pierce, T. E., Puxbaum, H., Shearer, M., Skiba, U., Steinbrecher, R., Tarrason, L., and Öquist, M. G.: Inventorying emissions from nature in Europe, J. Geophys. Res., 104, 8113–8152, 1999.
Sofiev, M., Vankevich, R., Lotjonen, M., Prank, M., Petukhov, V., Ermakova, T., Koskinen, J., and Kukkonen, J.: An operational system for the assimilation of the satellite information on wild-land fires for the needs of air quality modelling and forecasting, Atmos. Chem. Phys., 9,

ACPD
12, 3467–3507, 2012

6833–6847, doi:10.5194/acp-9-6833-2009, 2009.
Steinbrecher, R., Smiatek, G., Köble, R., Seufert, G., Theloke, J., Hauff, K., Ciccioli, P., Vautard, R., and Curci, G.: Intra- and inter-annual variability of VOC emissions from natural and semi-natural vegetation in Europe and neighbouring countries, Atmos. Environ., 43, 1380–1391, 2009.
Stohl, A., Berg, T., Burkhart, J. F., Fjae'raa, A. M., Forster, C., Herber, A., Hov, Ø., Lunder, C., McMillan, W. W., Oltmans, S., Shiobara, M., Simpson, D., Solberg, S., Stebel, K., Ström, J., Trseth, K., Treffeisen, R., Virkkunen, K., and Yttri, K. E.: Arctic smoke – record high air pollution levels in the European Arctic due to agricultural fires in Eastern Europe in spring 2006, Atmos. Chem. Phys., 7, 511–534, doi:10.5194/acp-7-511-2007, 2007.
Treffeisen, R., Tunved, P., Ström, J., Herber, A., Bareiss, J., Helbig, A., Stone, R. S., Hoyningen-Huene, W., Krejci, R., Stohl, A., and Neuber, R.: Arctic smoke – aerosol characteristics during a record smoke event in the European Arctic and its radiative impact, Atmos. Chem. Phys., 7, 3035–3053, doi:10.5194/acp-7-3035-2007, 2007.
Trentmann, J., Andreae, M. O., and Graf, H.-F.: Chemical processes in a young biomass-burning plume, J. Geophys. Res., 108, 4705, doi:10.1029/2003jd003732, 2003.
Ulevicius, V., Byčenkienė, S., Remeikis, V., Garbaras, A., Kecorius, S., Andriejauskienė, J., Jasinevičienė, D., and Mocnik, G.: Characterization of pollution events in the East Baltic region affected by regional biomass fire emissions, Atmos. Res., 98, 190–200, 2010.
Westerling, A. L., Hidalgo, H. G., Cayan, D. R., and Swetnam, T. W.: Warming and Earlier Spring Increase Western U.S. Forest Wildfire Activity, Science, 313, 940–943, doi:10.1126/science.1128834, 2006.
Wotawa, G. and Trainer, M.: The Influence of Canadian Forest Fires on Pollutant Concentrations in the United States, Science, 288, 324–328, doi:10.1126/science.288.5464.324, 2000.
Yokelson, R. J., Bertschi, I. T., Christian, T. J., Hobbs, P. V., Ward, D. E., and Hao, W. M.: Trace gas measurements in nascent, aged, and cloud-processed smoke from African savanna fires by airborne Fourier transform infrared spectroscopy (AFTIR), J. Geophys. Res., 108, 8478, doi:10.1029/2002jd002322, 2003.

ACPD
12, 3467–3507, 2012

Table 1. Statistical performance for O_3 over all rural background monitoring stations of the EMEP network (stations of Northern Europe/stations of Central Europe). All the predicted-observed pairs are considered.

	Reference run NO_x/CO = 0.06	NO_x/CO = 0.025
Average		
Average predicted (ppb)	36.3 (35.8/35.9)	38.9 (41.6/36.6)
Average observed (ppb)	44.9 (44.0/45.4)	44.9 (44.0/45.4)
MNB (%)	−2.70 (−5.34/−0.13)	2.09 (5.37/0.94)
MFB (%)	−20.06 (−23.12/−19.79)	−14.07 (−9.80/−18.41)
MNE (%)	40.35 (39.99/44.27)	39.22 (37.64/43.87)
MFE (%)	36.63 (40.08/36.82)	33.39 (32.89/36.07)
RMSE (ppb)	17.44 (18.37/17.74)	16.17 (15.86/17.25)
Peak		
Peak normalized bias time-paired (%)	−34.98 (−33.77/−36.82)	−27.26 (−24.61/−28.44)
Peak normalized error time-paired (%)	34.98 (33.77/36.82)	28.42 (26.16/29.55)
Peak normalized bias time-unpaired (%)	−18.17 (−15.12/−20.73)	−7.04 (4.73/−13.82)
Peak normalized error time-unpaired (%)	19.37 (16.09/21.99)	20.28 (23.0/18.41)

ACPD
12, 3467–3507, 2012

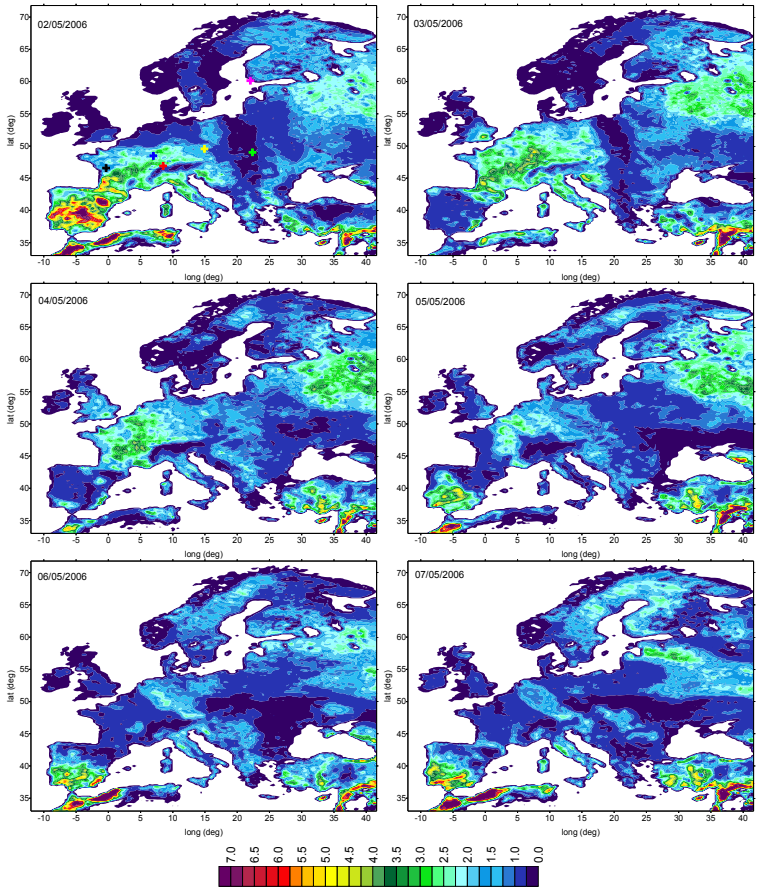

Fig. 1. Daily BVOC emission rates (mg m^{-2} day^{-1}) estimated with MEGAN for 2 to 7 May 2006. The symbols in the first plot correspond to monitoring stations measuring isoprene (red: CH0005; black: FR0015; blue: FR0008; yellow: CZ0003; magenta: FI0009; green: SK0006).

ACPD
12, 3467–3507, 2012

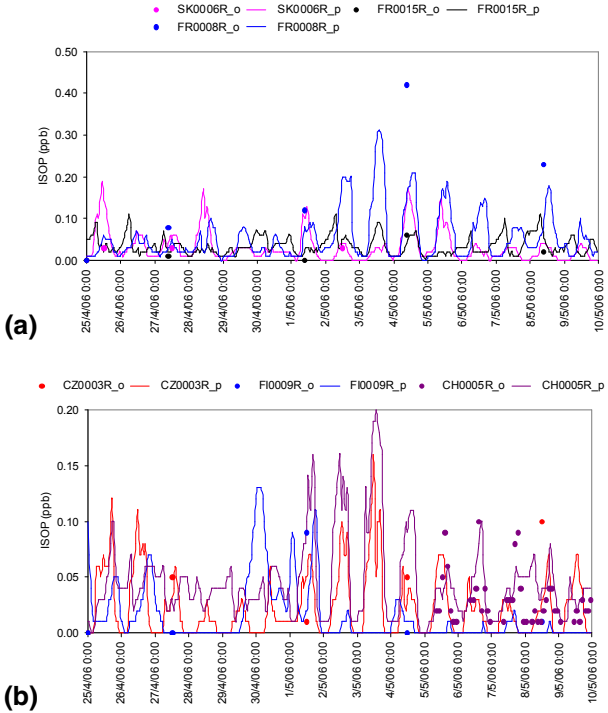

Fig. 2. Time series of predicted (lines) and observed (symbols) surface isoprene concentrations (ppb) during the simulation period at six stations of the EMEP network. The location of the stations is presented in Fig. 1 (upper left plot).

ACPD
12, 3467–3507, 2012

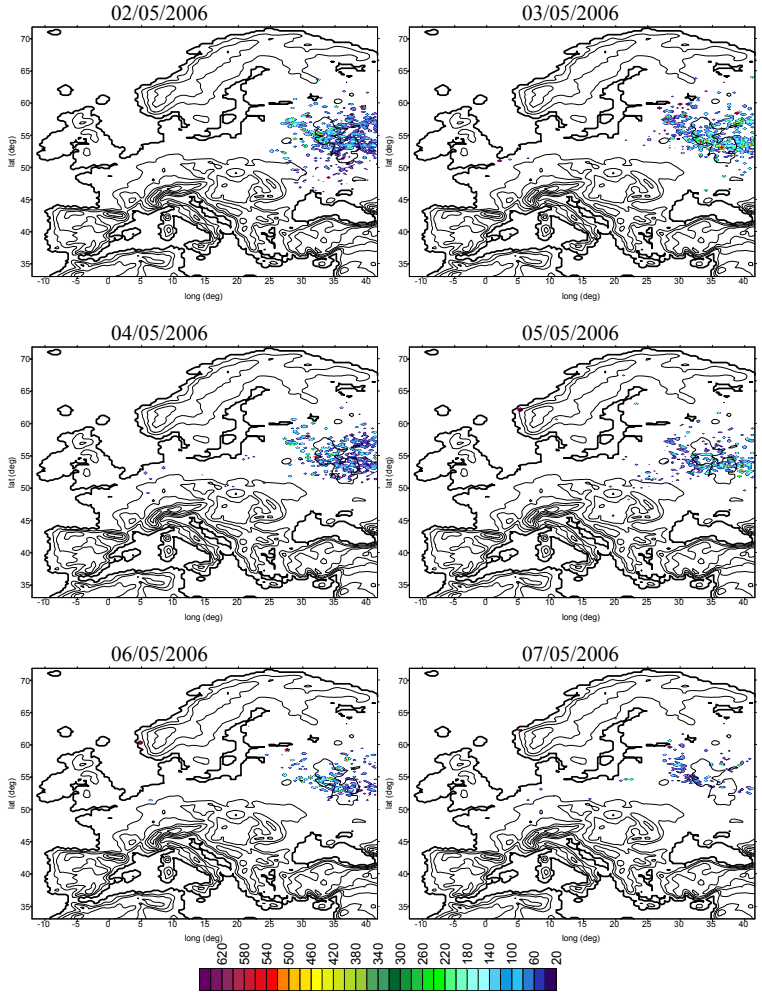

Fig. 3. Daily NO_x emissions (t) originated from fires during the period 2 May–7 May 2006.

ACPD
12, 3467–3507, 2012

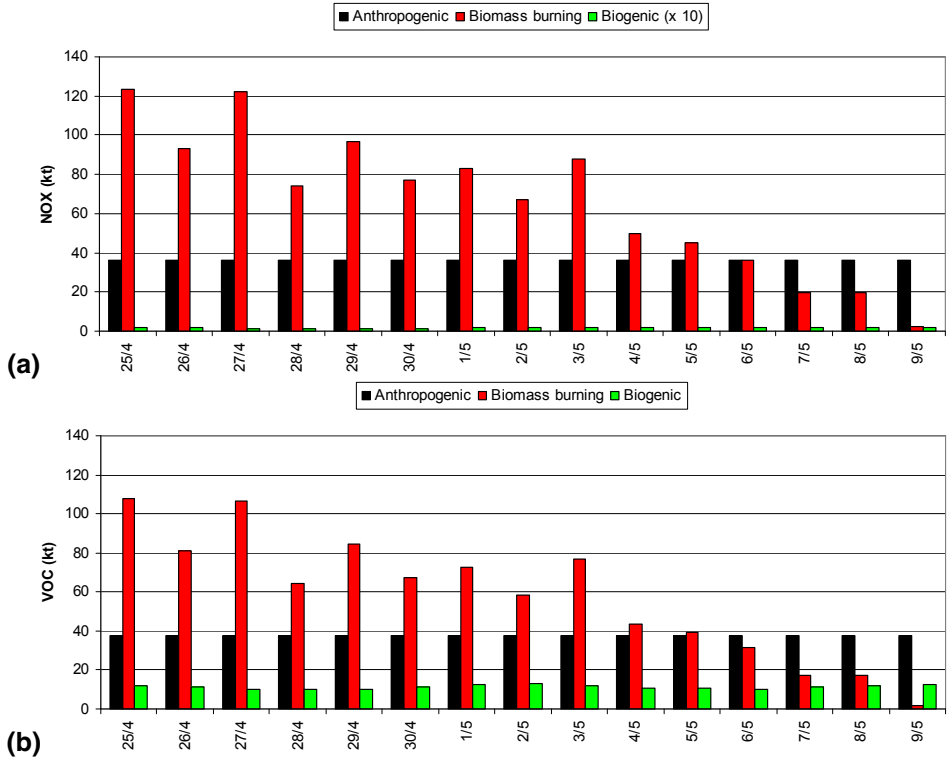

Fig. 4. Anthropogenic, biomass burning and biogenic NO_x and NMVOC emissions released over Europe during the simulation period.

ACPD
12, 3467–3507, 2012

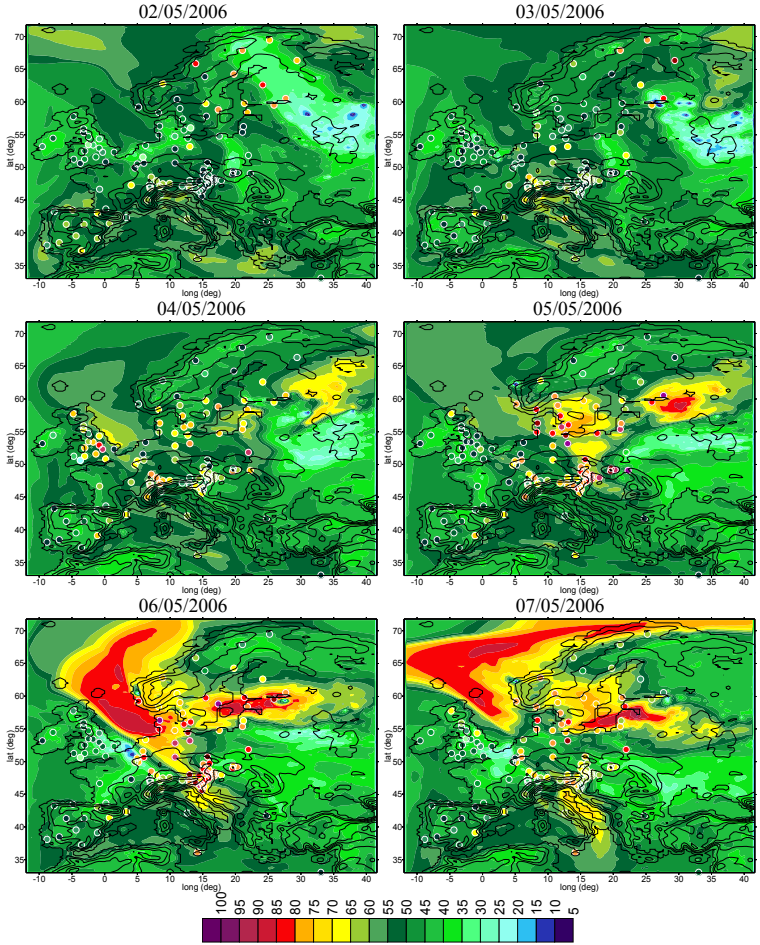

Fig. 5. Predicted (color shade) and observed (symbols) daily maximum mean hourly O_3 concentrations (ppb) during 2 May–7 May 2006.

ACPD
12, 3467–3507, 2012

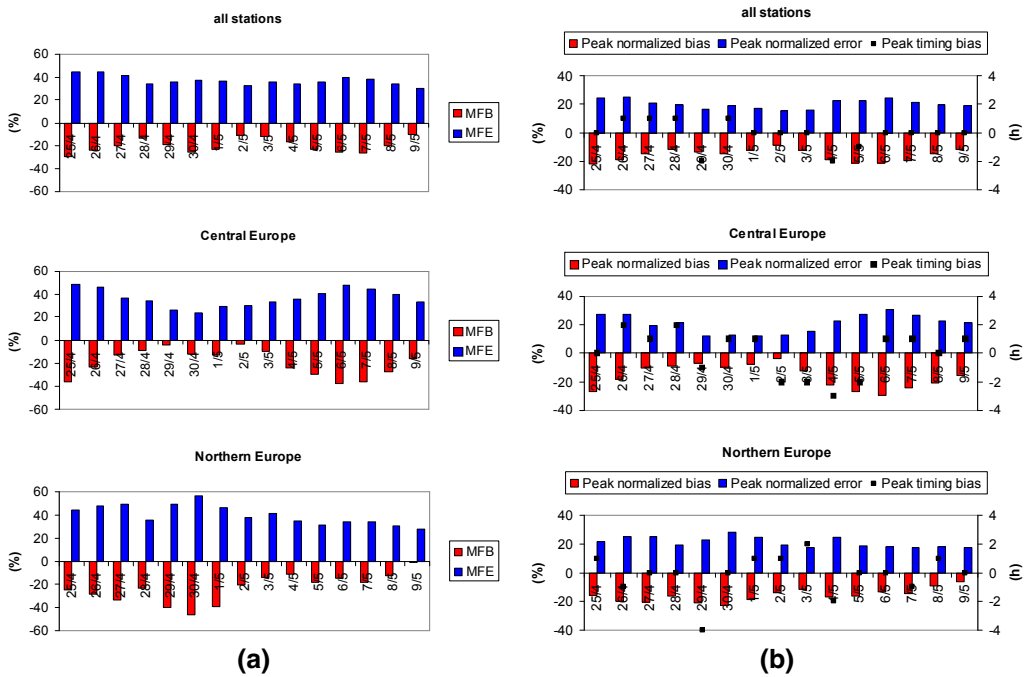

Fig. 6. Daily variation of the **(a)** MFB and MFE and **(b)** unpaired peak normalized bias, unpaired peak normalized error (left axis) and bias in peak timing (right axis) over all stations, and stations of Central and Northern Europe, during the period 25 April–9 May.

ACPD
12, 3467–3507, 2012

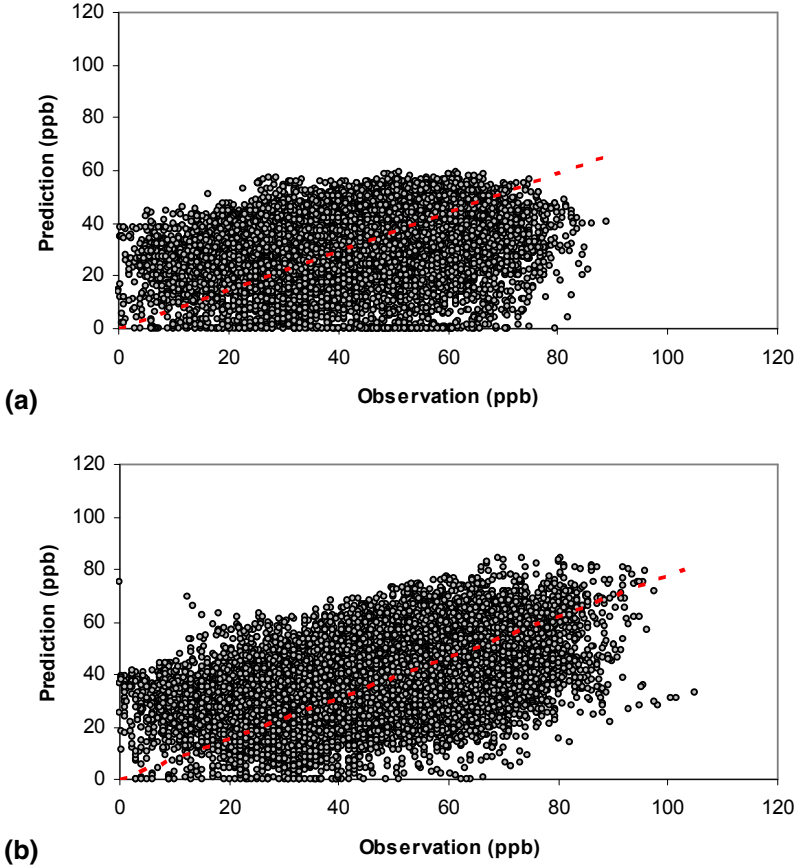

Fig. 7. Predicted and observed mean hourly O_3 concentrations over all stations for the periods: **(a)** 25 April–1 May and **(b)** 2–9 May.

ACPD
12, 3467–3507, 2012

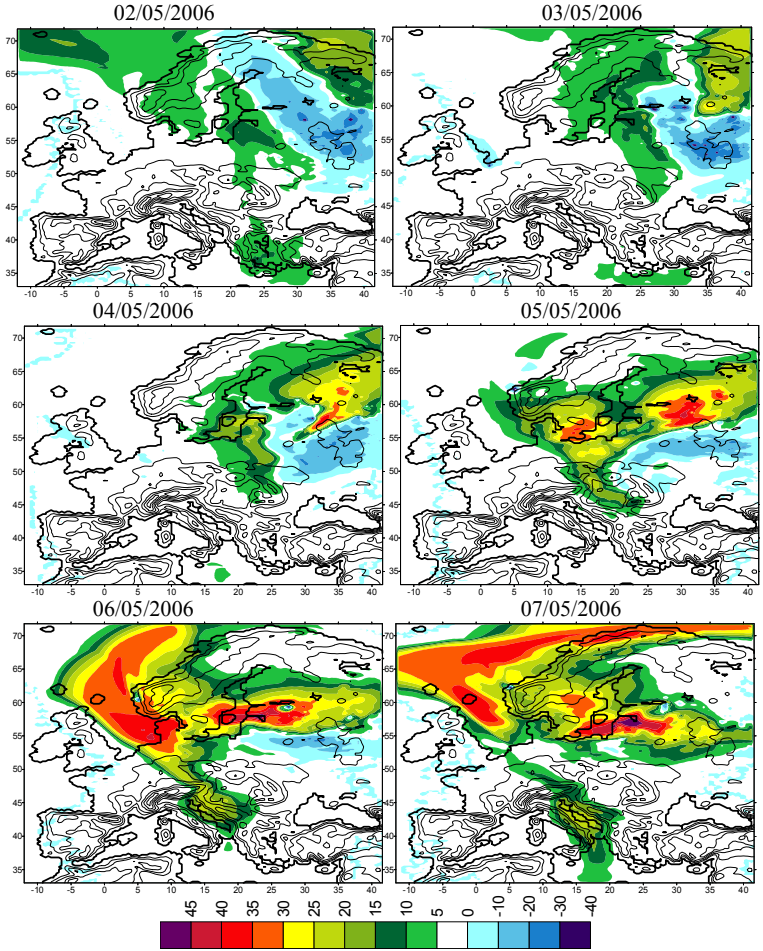

Fig. 8. Maximum impact of biomass burning emissions on mean hourly surface O_3 (ppb) during the period 2 May–7 May 2006. (Reference-NoFIRES).

ACPD
12, 3467–3507, 2012

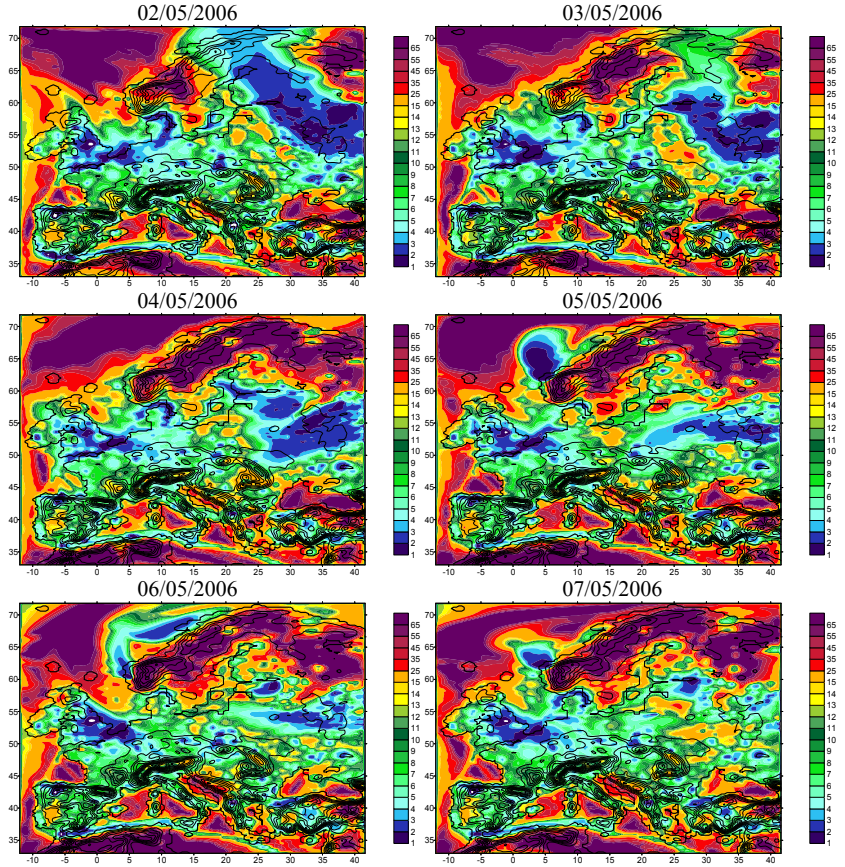

Fig. 9. Simulated VOC/NO_x ratios (ppbC ppb^{-1}) during 2 May–7 May 2006, at 12:00 UTC.

ACPD
12, 3467–3507, 2012

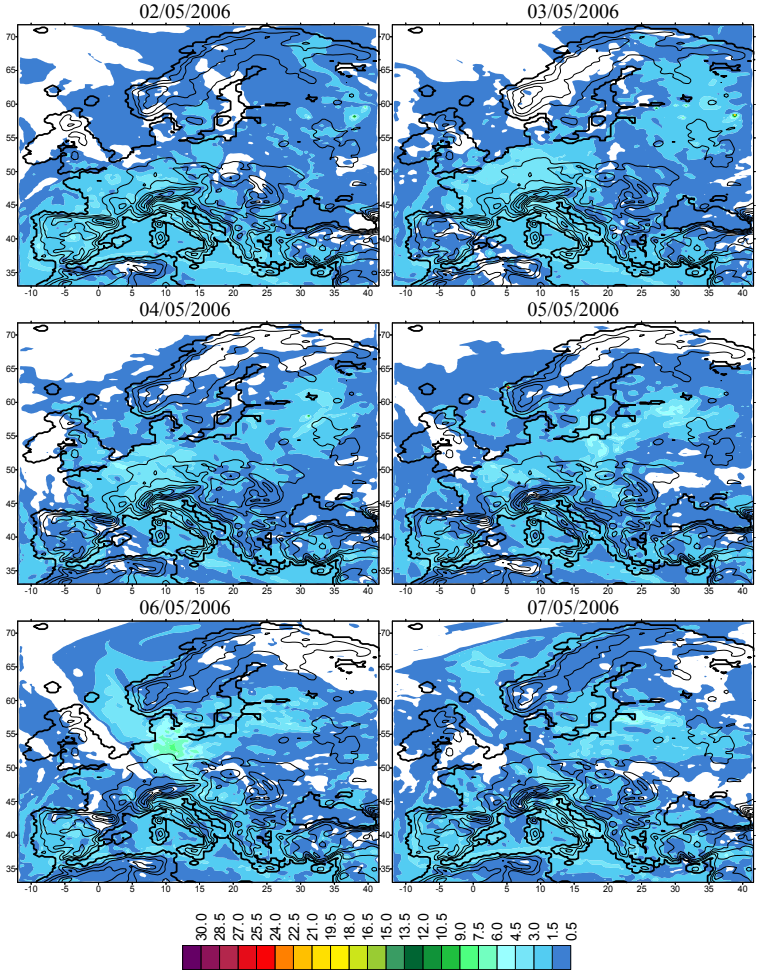

Fig. 10. Integrated hourly VOC (CO and CH_4 are included) – OH oxidation rates (ppb h^{-1}) during the period 2 May–7 May 2006, at 12:00 UTC.

ACPD
12, 3467–3507, 2012

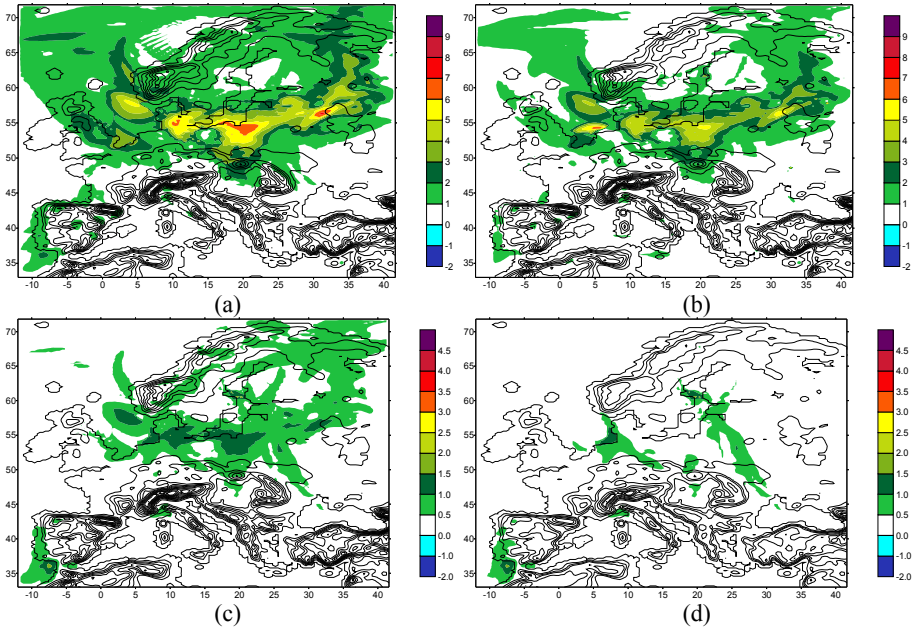

Fig. 11. Maximum impact on mean hourly surface O_3 (ppb) from **(a)** total BVOC, **(b)** isoprene, **(c)** terpenes and **(d)** BOVOC emissions.

ACPD
12, 3467–3507, 2012

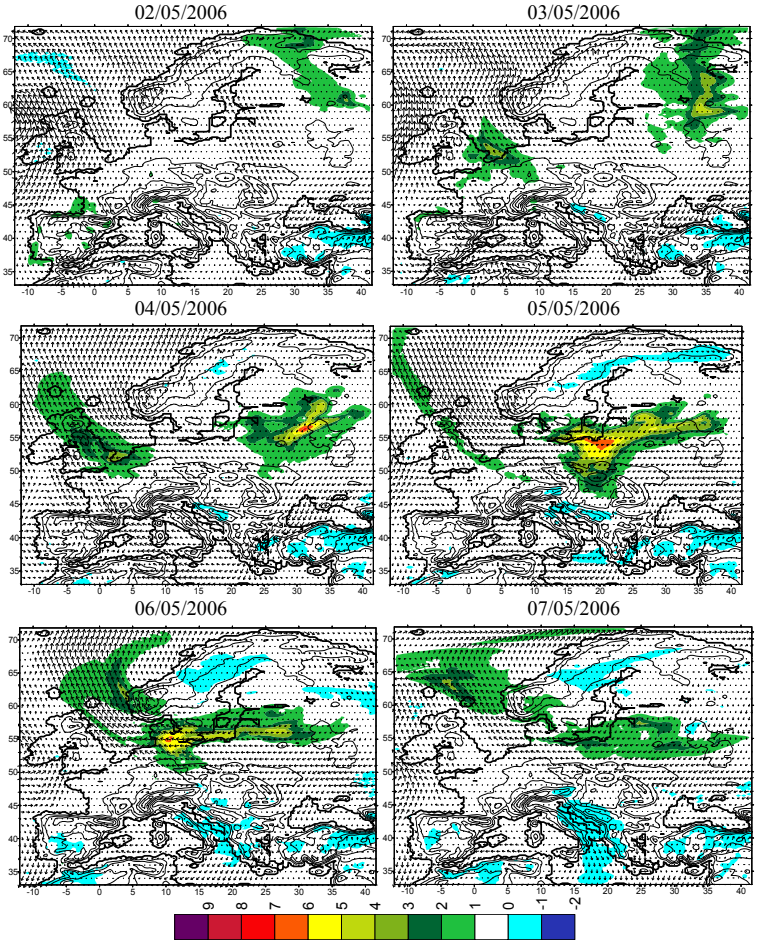

Fig. 12. Impact of total BVOC emissions on mean hourly surface O_3 (ppb) during the period 2 May–7 May 2006, at 12:00 UTC. The wind flow at 12:00 UTC is shown.

ACPD
12, 3467–3507, 2012

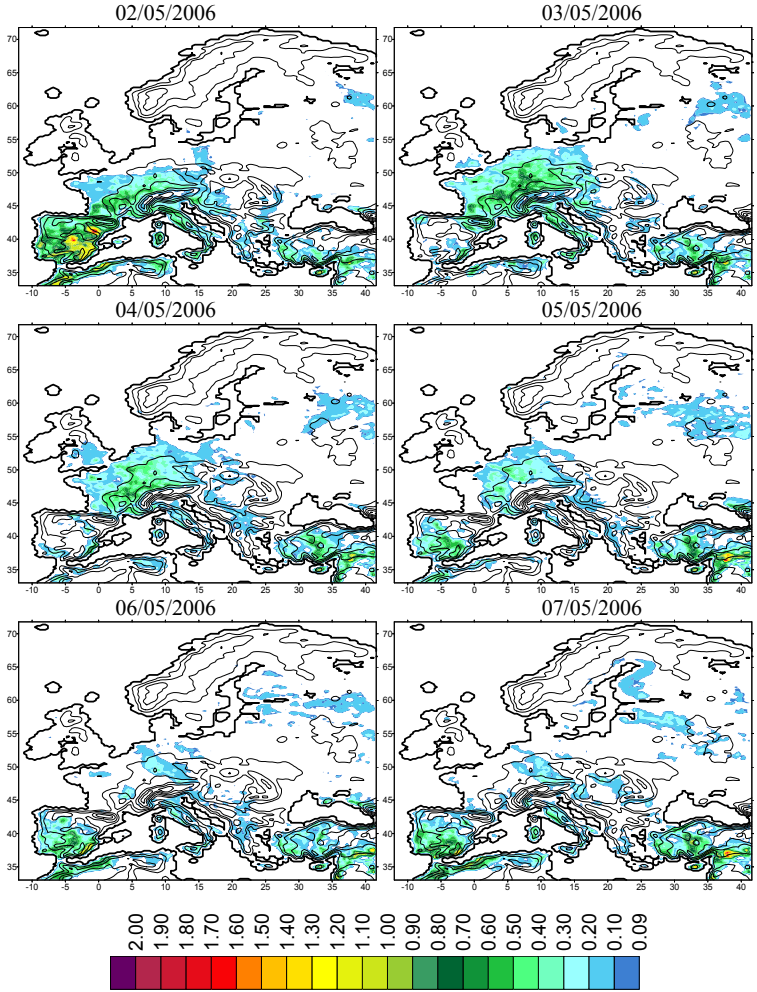

Fig. 13. Integrated hourly isoprene – OH oxidation rates (ppb h^{-1}) during the period 2 May–7 May 2006, at 12:00 UTC.

ACPD
12, 3467–3507, 2012